SSRG International Journal of Civil Engineering
ISSN: 2348-8352/ https://doi.org/10.14445/23488352/IJCE-V13I5P112

Volume 13 Issue 5, 172-186, May 2026

Original Article

Weathering-Controlled Transition of Slope Failure Mechanisms and Applicability of Kinematic Models in Silurian Schists (Rif, Northern Morocco)

MEROUANI Houda[1*], DEKAYIR Abdellilah[1], ROUAI Mohamed[1], EL BALGHITI Youssef[2]

[1]*Geoexploration and Geotechnics Research Team, Department of Geology, Faculty of Sciences, Moulay Ismail University, PB11201 Zitoune, Meknes, Morocco.*
[2]*Civil Engineering and Construction Structure GCC laboratory, Mohammadia School of Engineers, Mohammed V University, Rabat, Morocco.*

**Corresponding Author : h.merouani@edu.umi.ac.ma*

Received: 14 January 2026 Revised: 20 February 2026 Accepted: 11 March 2026 Published: 29 May 2026

Abstract *- Paleozoic schist on the Mediterranean road in northern Morocco presents a transition in slope stability from discontinuity-controlled to soil-like behavior. This phenomenon is related to the complex mechanical behavior shown under the effects of weathering processes. The present study investigates this transition in the Silurian schist on a slope near Tamrabet (northern Morocco). After field observations, six weathering zones were identified to define the critical changes between partially interbedded rock and heavily degraded matrix material. The findings of the petrographic, mineralogical, and geotechnical characterization together describe the progressive effects of weathering shown in the increasing porosity, decreasing bulk density, loss of mineral crystallinity, and leaching of mobile elements, which result in a significant contraction of the rock fabric, accompanied by swelling in the soil-like material resulting from weathering. The stability behavior of the slope mirrored the effect of this degradation on mechanical behavior. Kinematics models were used as a verification tool and systematically compared with instabilities observed in the field, highlighting both their relevance and their limitations. This comparison makes it possible to differentiate between rocky areas where instability is governed by the geometry of discontinuities and can be assessed using kinematic approaches, and heavily weathered areas where the behavior of the low-cohesion matrix controls the failure mechanisms that cannot be considered by these models. Overall, the results reveal the existence of a mechanical limit within the schist weathering profile and provide a comprehensive approach for soft-rock stability assessment in the transition phase between rock and soil.*

Keywords *- Schist, Rock–soil transition, Slope stability, Weathering, Geomechanics.*

1. Introduction

The Moroccan Rif is highly susceptible to instabilities resulting from a combination of natural factors, namely geological complexity and steep relief, and significant anthropogenic intervention in the context of the region's socio-economic development. This high vulnerability has a significant impact on infrastructure, particularly National Road No. 16, a strategic transport axis in the region. Recurring instabilities pose a major challenge in terms of public safety and infrastructure management.

Numerous studies conducted in the Rif region[1-3] have focused on inventorying, mapping, and assessing susceptibility to ground movements, as well as on the geological and structural characterization of specific sites [4-6]. Although these studies have emphasized the mechanical properties of materials on slope stability and the influence of precipitation [7, 8], or have applied various methodological approaches ranging from susceptibility mapping and multifractal analysis to risk assessment frameworks that consider potential socio-economic impacts [9-11].

Paleozoic schists, classified as soft rocks [12], are among the formations most susceptible to instability due to their pronounced anisotropy, high weatherability, and relatively low mechanical strength. Experimental studies have shown that the influence of structural anisotropy on failure mechanisms strongly depends on the mechanical state of the material and tends to decrease as the material becomes progressively degraded [13, 14].

Under surface conditions, low normal stresses, sensitivity to water, and the presence of thin, weak facies further complicate mechanical characterization. These conditions make conventional strength tests difficult to implement and often poorly representative of the actual behavior of slopes composed of weathered schists [15, 16]. Similar observations have been reported in studies on weak rock formations, where significant transfer of weathering-induced rock mass characteristics in the mechanical response and failure, especially in soft and anisotropic lithologies [12, 17].

In the literature, weathering profiles in schistose structures have been described as a series of states ranging from intact bedrock to residual soil, often associated with the process of mineralogical weathering [18, 19]. The progressive change is manifested by transitional rock–soil behavior for which the decomposed matrix controls the geomechanical response progressively more than discontinuities.

The progressive change is manifested by transitional rock–soil behavior for which the decomposed matrix controls the geomechanical response progressively more than discontinuities. From an engineering perspective, mechanical transition is often associated with a value of 1 MPa or less of uniaxial compressive strength, under which the material behaviour is assumed to become soil-like [18, 20].

The assessment of the stability of slopes affected by weathering is often based on rock mass classification systems. [20], supported with monitoring instruments such as inclinometers and piezometers for detecting progressive deformation and hydrological effects [21, 22]. Such observations are consistent with other studies of how water–rock interactions activate weathering processes and drive slope instability in schist formations [19].

The transition of mechanical behavior is a frequent phenomenon in schist slopes, where instability mechanisms evolve from rupture controlled by the geometry of discontinuities to instabilities controlled by the weathered matrix. These intermediate behavior combination types and outputs do not easily fit the criteria associated with conventional stability approaches developed for intact rock masses primarily governed by discontinuity features or soils governed by continuum mechanical behavior.

Despite the abundance and importance of research devoted to instabilities in the Rif region, the mechanical changes undergone by materials under the effect of progressive weathering remain insufficiently considered in slope stability assessments. In concrete terms, few studies have clearly examined the changes resulting from weathering on the relative influence of discontinuities and matrix degradation on instability mechanisms.

Therefore, this study aims to understand how progressive weathering in schists modifies the mechanical behavior of slopes, in addition to identifying the transition between discontinuity-controlled failures and matrix-controlled failures, beyond the applicability of traditional kinematic models.

The study was implemented in a slope of the Tamrabet region on the Mediterranean coastal road (National Road No. 16), where Silurian schists show a strong mechanical transition associated with weathering processes. To explore this transition, we adopt a multidisciplinary approach that integrates field observations, physical, geochemical, and petrographic analyses with kinematic analysis employed as a geometric admissibility test. This novel integrated framework allows for a better description of the mechanical evolution of weathered schists and enhances the knowledge on the mechanisms of instability at rock–soil transitional domains.

The present study contributes to improving the understanding of instability mechanisms in weathered schist slopes by:

(i) characterizing the progressive evolution of physical, geochemical, and petrographic properties along a weathering profile;
(ii) identifying the transitional mechanical domain between rock-like and soil-like behavior in schist formations;
(iii) and integrating weathering indicators with kinematic analysis to evaluate the geometric admissibility of structurally controlled slope failures.

This approach provides insights into the role of progressive weathering in modifying instability mechanisms in weak anisotropic rock masses.

2. Study Area

The Tamrabet site (X = 35.5300, Y = -5.1967) is located approximately 25 km from Tetouan, within the Akaili nappe of the Ghomarides unit, on the side valley crossed by the National Road N°16, between Ras Timezzourega and Ras Akaili. The studied area is situated on the Silurian formation, which consists of lustrous clayey schists and conglomerates containing elongated quartz clasts [23].

During road construction between 2009 and 2012, the Tamrabet site was excavated, exposing schist that records successive Eo-Variscan (D1–D2), Variscan (D3), and Alpine deformation phases. These successive events introduced a general structural framework, including early subhorizontal schistosity with NNE-oriented folds (D1), crenellated schistosity and inclined NE-trending folds with microfolds and stretch lineations (D2), followed by late EW shear planes that underwent local reactivation during alpine epizonal metamorphism [5]. Due to the different angles of intersection between the schistosity and joint networks, heterogeneous geometric conditions exist along the slope, as the site was excavated with curved road sections and moderate to steep slopes.

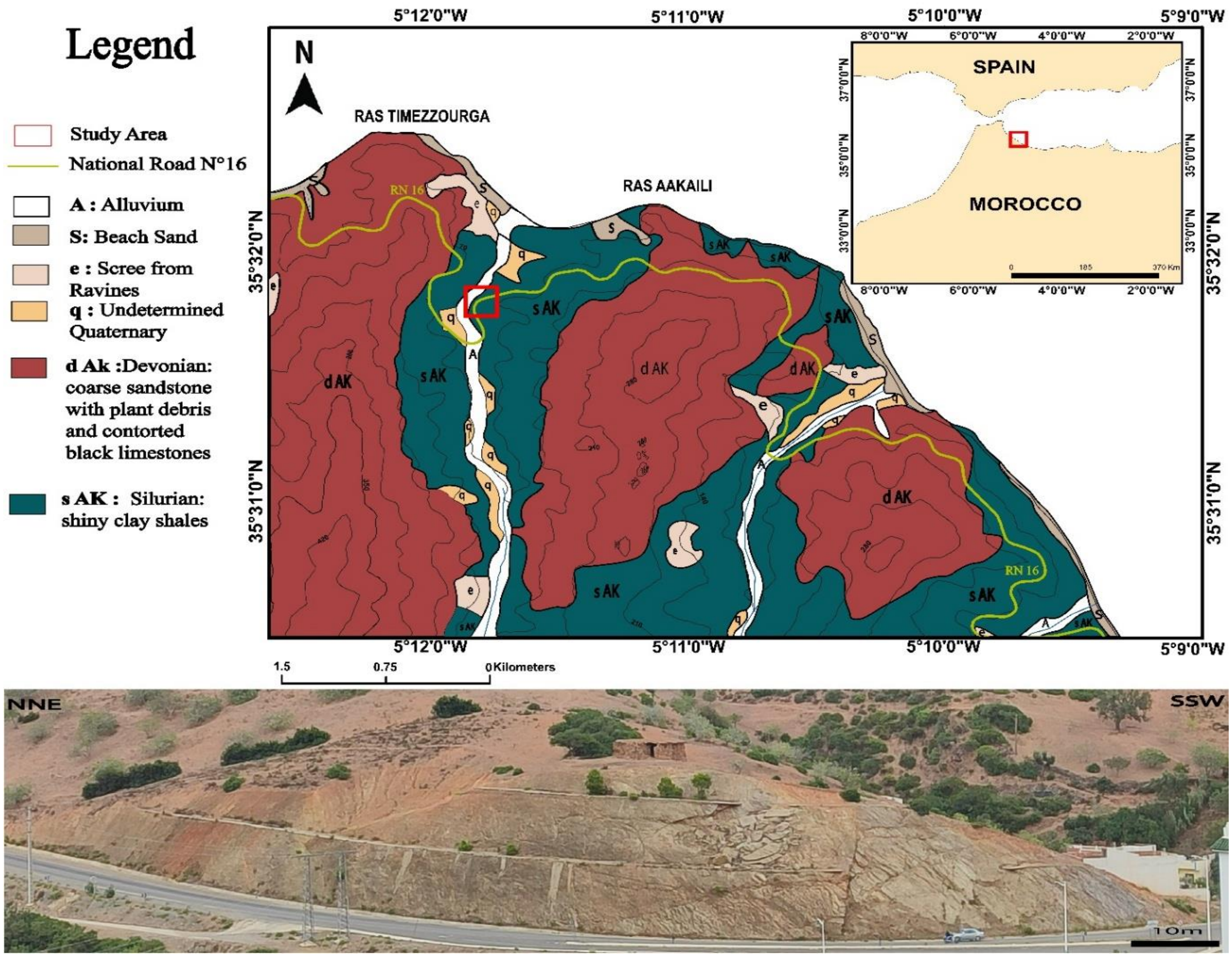

Fig. 1 The studied area of the Tamrabet site, on the geological map of the region, redrawn [24, 25]

The Silurian schist is mainly composed of quartz, mica, and sericite, with minor feldspar, chlorite, and iron oxides, and is characterized by a color of dark gray to black [4]. This mineralogical assemblage, dominated by phyllosilicates, favors progressive weathering of the rock mass under surface conditions.

The slope exposed an in-situ weathering profile, with no evidence of significant material transport, and revealed a marked lateral variability in weathering intensity. This variability results in the juxtaposition of different weathering states over short distances, leading to the coexistence of rock-dominated and matrix-dominated materials along the same slope.

3. Materials and Methods

The methodology follows a stepwise approach, combining field-based weathering characterization at outcrop and specimen scales and probabilistic kinematic modelling to identify the weathering-controlled limits of applicability of structure-based slope failure models. The approach is hypothesis-driven: mechanical behavior is assumed to be constant as fully rock-based across the entire slope, and the resulting kinematic predictions are systematically compared with the different failure mechanisms observed under progressive weathering as a variable reference.

3.1. Field and Laboratory Characterization

Seventeen samples were then collected from a carefully chosen weathering profile that was representative of the progressive variability of weathering across this slope. Two complementary scales were studied: the outcrop scale, linked to the rock mass, where geotechnical and geological studies make it possible to delineate areas of weathering and document associated slope instabilities, and the sample scale, where the weathering state of the material was characterized using a series of indices established in the laboratory. This multi-scale framework provides a consistent description of the evolution of weathering in the Silurian shales of the Ghomaride unit.

At the outcrop scale, the study consisted of a systematic technical field survey along the road cut to define the weathering zones, structural features, and slope instabilities.

3.1.1. Weathering Zoning

Weathering zones are rock masses, in situ rocks with their discontinuities and weathering [20], classified according to the progression of weathering. In the field, weathering zones are mapped, and the boundaries between them are defined using observable criteria, including the condition of discontinuities, the preservation of rock structure, and the relative proportion of soil and core rocks.

This weathering profile, obtained from the evaluation of rock masses, is more effective for engineering applications and mapping [25].

3.1.2. Classification of Slope Instabilities

Slope instabilities were systematically mapped along the outcrop via direct field inspection. Identification was based on observable geomorphological and structural characteristics, including rupture surface geometry (planar versus curved), surface orientation, direction of displacement, daylighting discontinuities, block detachment features, and evidence of deformation within the matrix.

For each instability, the rupture surface orientation and its relationship to the mapped discontinuity sets were recorded. The spatial position of each feature was documented relative to slope orientation and previously defined weathering zones. Instabilities are categorized based on the slide type using the Varnes system [26].

Classification into subclasses was based only on in-situ structural relationships between rupture geometry, which enabled us to distinguish between structurally controlled failures and matrix-dominated deformation structures.

In addition, it was ensured that only features that were clearly identifiable and geometrically interpretable with respect to failure were kept for the purpose of mapping. The consistency between the observed failure surfaces and the orientations of the discontinuities measured with the slope geometry was used to cross-check the interpretations in the field.

In addition, the elements of instability were recorded using sketches made in the field and photographs, which will facilitate subsequent verification and interpretation. In this way, the mapped instabilities could be compared with kinematic predictions with a minimum of observational uncertainty.

3.1.3. Structural Measurements

On the outcrop, structural features were identified in sets, and orientation measurements were obtained using a geological compass at representative and structurally well-defined locations across the slope. Care was taken to avoid weathered, irregular, or ambiguous surfaces. Repeated measurements were performed where necessary to verify consistency. The resulting orientation datasets (n = 247) were statistically treated using Fisher distributions to account for natural dispersion within each discontinuity set.

3.1.4. Schmidt Hammer Test

The Schmidt Hammer (SH) was employed [27] due to the difficulty of obtaining test samples suitable for conducting mechanical property tests. Using a standard impact energy of 2.207J, the rebound hammer index (R) was measured according to the needle indicator system and given in descending order. A test area of about 20 × 20 cm was chosen at each measurement location, to which twenty strikes of the hammer were applied in a direction perpendicular to the foliation.

Schmidt hammer measurements were repeated at multiple locations within the different weathering zones identified at the outcrop scale. Outlier impacts were discarded following standard rebound testing protocols to ensure consistency of rebound values.

To visualize the spatial relationships between the mapped instability, structure preservation, and the weathering zone, simplified representations of these features on the slope have been made.

To complement this outcrop-scale characterization, specimen analysis spatially correlated with the mapped weathering zones in a way that each zone encompasses one or more specimen-scale weathering grades.

At the specimen scale, a series of test indices was performed to characterize weathering-related changes in physical, geochemical, and micro-petrographic properties, using the least weathered sample as a reference [28].

3.1.5. Weathering Grades

At the specimen scale, weathering grades were determined based on macroscopic observations and geological hammer testing following ISRM recommendations [29].

3.1.6. Physical Analysis: Density and Porosity

The physical properties of the seventeen schist samples were investigated by determining the total porosity by combining the paraffin-coated hydrostatic weighing method for bulk density (ρ_b) with the pycnometer method for absolute (true) density (ρ_t), following the AFNOR standards [30, 31]. Total porosity was calculated from the ratio of bulk to true density. For each sample, bulk and true density measurements were performed in triplicate. The reported values correspond to the mean of three subsamples, and measurement consistency was verified before total porosity calculation.

3.1.7. Geochemical Analysis: Mass and Volume Change

A set of representative samples was analyzed for chemical composition using a wavelength-dispersive spectrometer at the CNRST-UATRS. An isochemical mass balance approach was applied, using zirconium (Zr) as an immobile reference element [32]. Relative mass transfer coefficients and volume change parameters were calculated to assess elemental gains and losses relative to the least weathered reference sample.

Analytical precision was monitored through standard calibration procedures at the CNRST-UATRS laboratory. Sample preparation using an agate mortar minimized contamination. The use of zirconium (Zr) as an immobile element was validated by its consistent behavior across the weathering profile.

3.1.8. Petrographic Analysis

Thin sections were prepared from representative samples of the weathering profile, excluding highly disaggregated material. The Micropetrographic Index (Ip) [33], as the ratio between the percentage of the area of sound constituents to that of unsound constituents, allows quantifying microstructural changes related to weathering.

Optical microscope observations in polarized light were carried out with image analysis using the Trainable Weka Segmentation plugin in FIJI, employing manually labeled examples from weathered and unweathered features to train a model for automated classification.

The analysis was based on three independent thin-section images of each sample, and the final IP value corresponds to the average of these measurements. Variability between images was considered to ensure analytical consistency.

3.1.9. Data Analysis

The data of physical (porosity, bulk density), Geochemical (Mass and volume change), micropetrographic (Ip), and rebound index were all analysed according to weathering grades and zones. Between two and six independent samples were tested per weathering grade. sample means were derived, from which mean values and standard deviations were calculated to describe the variability within each grade.

Regarding the restricted number of samples per weathering grade, comparisons were undertaken descriptively; the focus was on progressive trends and determination of threshold behaviour rather than formal inferential statistical testing. Variability is shown in figures using standard deviation error bars. Geochemical mass balance calculations were made using zirconium as an immobile element in reference to the least weathered reference sample.

3.1.10. Quality Control and Reproducibility

Laboratory measurements were performed according to established analytical methods. Porosity, bulk density, and micropetrographic index measurements were carried out in triplicate per sample to confirm analytical precision. Values given are means of multiple repeated measurements.

Powdered samples were prepared in a contamination-free manner for geochemical analyses, with spectrometric calibration according to laboratory standards at CNRST-UATRS.

To account for variability in Schmidt hammer readings, standardized field procedures were established, which included multiple impacts per test area. These procedures promoted internal consistency of the dataset prior to interpretation and ensured reproducibility.

3.2. Kinematic Analysis

The kinematic analysis was conducted as a geometrical admissibility assessment of structure-controlled slope failure. The approach was intentionally limited to geometric compatibility to isolate the role of structural configuration, independent of weathering-induced strength degradation. Accordingly, the slope was modeled under the simplifying assumption of fully rocky behavior, whereby potential instabilities are governed solely by discontinuity–slope orientation relationships.

A total of 247 discontinuity measurements were collected in the field. Four discontinuity sets were identified: S0–1 (primary schistosity, parallel to bedding), S2 (secondary schistosity), J1 (joints), and J2 (low-dip joints). These datasets provided the geometric input for probabilistic stereographic analysis.

To account for the longitudinal curvature of the slope, three representative orientations of the slope face were analyzed. Plane sliding and wedge sliding, which represent the predominant failure mechanisms controlled by the structure observed in the field, were evaluated to determine their kinematic admissibility. Other failure modes were not considered.

Admissibility criteria were based on classical geometric conditions such as daylighting requirements, dip-direction compatibility within a tolerance of ±20°, and friction angle limits. A conservative friction angle of 15° was used based on field observations. Results were reported based on admissible vs non-admissible kinematic conditions, rather than factors of safety. The proportion of discontinuity orientations in which the defined geometrical criteria were simultaneously satisfied was calculated as a measure of kinematic compatibility. Rocscience Dips software was used for stereographic projection and statistical analysis of failure probability.

The kinematic predictions were then compared with mapped instabilities within the delineated weathering zones to assess limits of applicability for purely structure-based, kinematic models under progressive weathering.

4. Results and Discussion

4.1. Slope Description

On-site investigations provide essential information about slope geometry and failure mechanisms. The curved shape of the road cut causes variations in the orientation of the slope faces, associated with a gradual loss of structural integrity due to weathering. The observed failure mechanisms vary along the slope from SSW to NNE, planar sliding along a dominant schistosity plane, wedge failure generated by the intersection of schistosity and joint sets, and localized rotational sliding in highly altered zones. In addition, minor block detachments are observed, particularly in areas of preserved structure, without evidence of slope-scale instability.

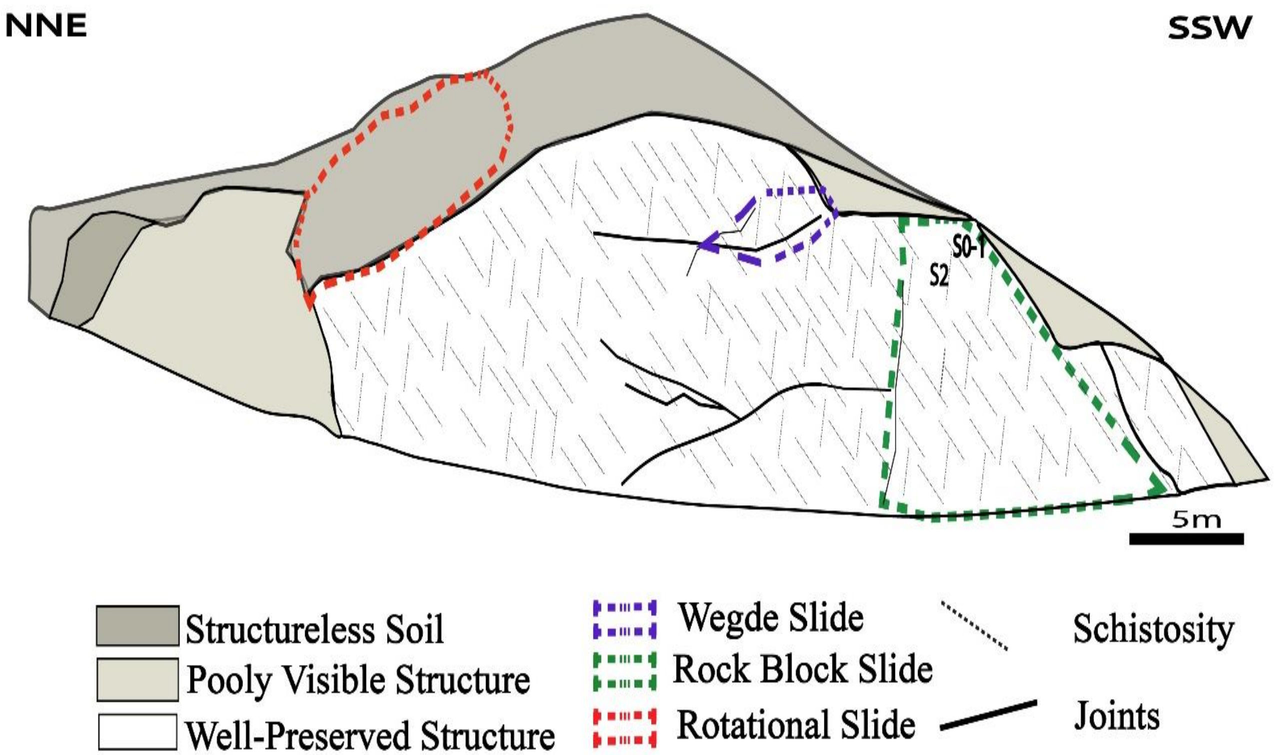

Fig. 2 Simplified representation of the studied slope showing the spatial distribution of failure mechanisms and the degree of structure preservation along the road cut

4.2. Outcrop-Scale Weathering Zoning and Spatial Distribution

The progression of weathering is the key factor controlling the variation observed in failure mechanisms across both different rock masses (outcrop) and material (specimen) scales.

At the outcrop scale, six weathering zones are delineated and carefully mapped. The boundary between zones 1 and 2 corresponds to the opening of discontinuities and the transformation of some plans into weak surfaces. In the higher zones, the relative proportions of soil and rock cores vary: in zone 3, soil is present in minor proportion, and the structure remains locked, while in zone 4, soil and rock proportions are roughly equivalent; in zones 5 and 6, the resulting soil progressively dominates the rock mass.

At the specimen scale, the sampled material from across the slope was classified into six weathering grades, from grade I (fresh rock) to grade VI (residual soil), based on macroscopic observations, including changes in color, foliation, and texture.

Superposition of weathering zones and material grades allows correlation between outcrop and specimen-scale weathering.

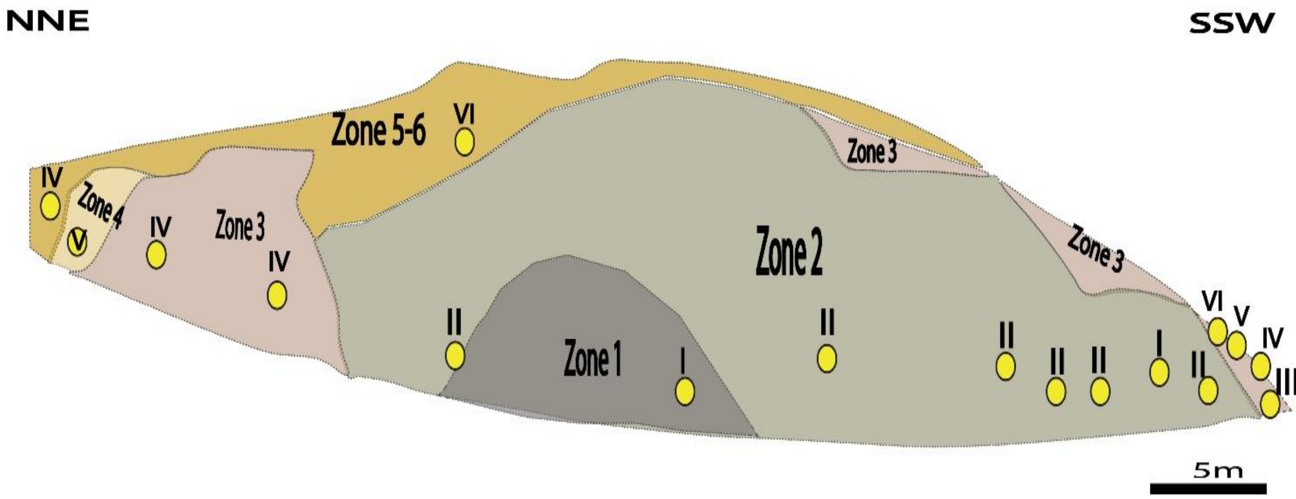

Fig. 3 The association of the two scales, outcrop and specimen, is shown in the representation of the spatial distribution of the weathering zones of rock masses and the weathering grades of material

4.3. Mechanical Degradation at the Outcrop Scale: The Rebound Hammer Index

The variation in the rebound index was recorded following predefined weathering zones along the outcrop. Surface hardness shows a systematic decrease with the increase in the degree of weathering.

The major trend of the rebound index evolution begins with a gradual decrease in weathering zones 1 to 3, due to the progressive degradation of the rock matrix. This indicates an increasing weakening of the rock structure due to mineral weathering, microfracturing, and increased porosity. In these zones, the average rebound values remain within the Schmidt hammer range but show increasing variability as weathering progresses.

Beyond zone 3, the index is impossible to measure ($R < 10$), indicating that weathering exceeds the effective operating range of the instrument.

In highly weathered or soil-like materials, the Schmidt hammer response becomes unreliable due to surface friability, energy dissipation within the degraded matrix, and the absence of the elastic rebound conditions required for meaningful measurements [27]. Consequently, values below R = 10 were not considered representative of rock mechanical behavior and were excluded from further quantitative interpretation.

In highly altered or soil-like materials, the response of the Schmidt hammer becomes unreliable due to the friability of the surface, energy dissipation in the degraded matrix, and the absence of the elastic rebound conditions necessary to obtain meaningful readings. Therefore, values below R = 10 were not considered representative of the mechanical response of the rock and were therefore excluded from any further quantitative interpretation.

A marked increase in the dispersion of rebound indices is observed in weathering zone 3. This increased variability is representative of the mechanical heterogeneity that characterizes transitional weathering domains, in which partially intact rock structures coexist with increasingly degraded matrix materials. Such dispersion is therefore considered to reflect transitional behavior in the weathering process [27].

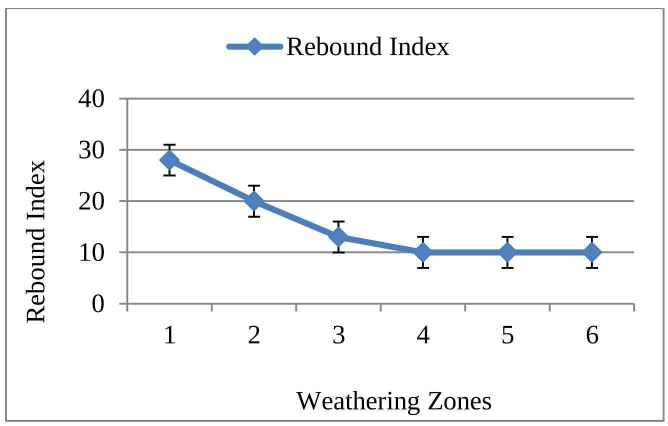

Fig. 4 Schmidt hammer rebound index variation across the weathering zones

4.4. Material-Scale Degradation with Weathering

The main purpose of specimen-scale analyses is to quantify and monitor the changes caused by weathering on the properties of the material, starting with intact rock and ending with residual soil.

Physical properties show systematic trends with increasing weathering grade. Porosity increases while bulk density decreases, reflecting progressive material loosening and structural breakdown. These trends progress gradually through weathering grades I to IV before being marked by a break point observed in the transition between grades V and VI, where the porosity reaches its highest values of 38%, and the bulk density drops abruptly, marking a mechanical and structural threshold in the weathering profile.

Grade IV shows marked variation in bulk density and total porosity, as indicated by a relatively high standard deviation. This variability probably stems from the heterogeneous development of fracture connectivity and mineral alteration at this intermediate stage of weathering. Although the samples are classified at the same grade, the degraded internal structure appears uneven, reflecting variable changes in porosity.

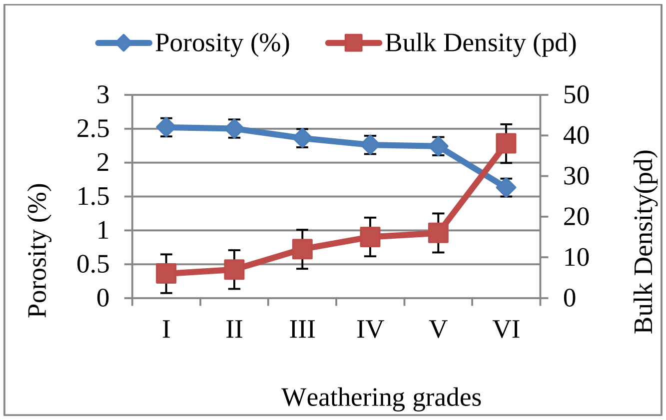

Fig. 5 Variation of porosity and bulk density across the weathering grades

The same trend is observed in petrographic degradation. The micropetrographic index decreases with increasing weathering, reflecting the progression of mineralogical alteration and texture disorganization. The index declines significantly from grade I to III, then gradually continues downwards through grade IV and V, finally reaching zero at grade VI — residual soil type in which the original rock fabric has been destroyed.

However, the standard deviation reveals that dispersion is significantly higher in grade II than in other grades. This dispersion likely reflects the heterogeneous onset of micro-alteration processes, which are not yet fully pronounced at the macroscopic scale. Despite macroscopic classification of samples into the same weathering grade, thin-section observations reveal varying degrees of mineral weathering and microfracturing, resulting in greater intra-grade variability.

Geochemical analyses show significant mass and volume changes as weathering progresses. The relative volume change is negative for all degrees of weathering except degree IV, indicating a loss of solid mass in the rock caused by the dissolution and leaching of soluble mineral phases; consequently, the volume gains by minerals neoformation and hydration in the resulting soil are represented by degree IV.

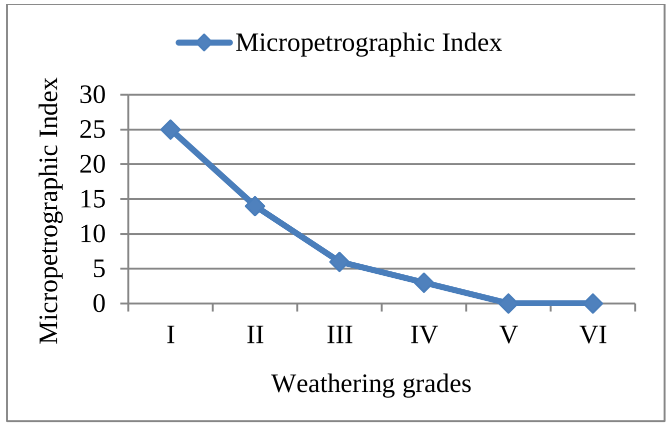

Fig. 6 Micropetrographic index changes across weathering grades

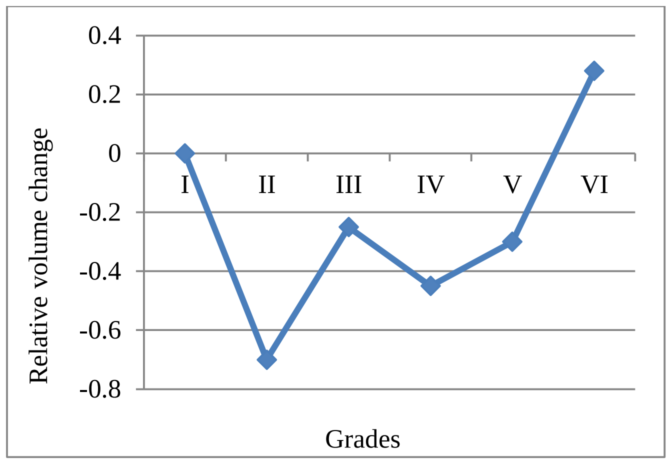

Fig. 7 The Relative volume changes across weathering grades, reported to the fresh rock

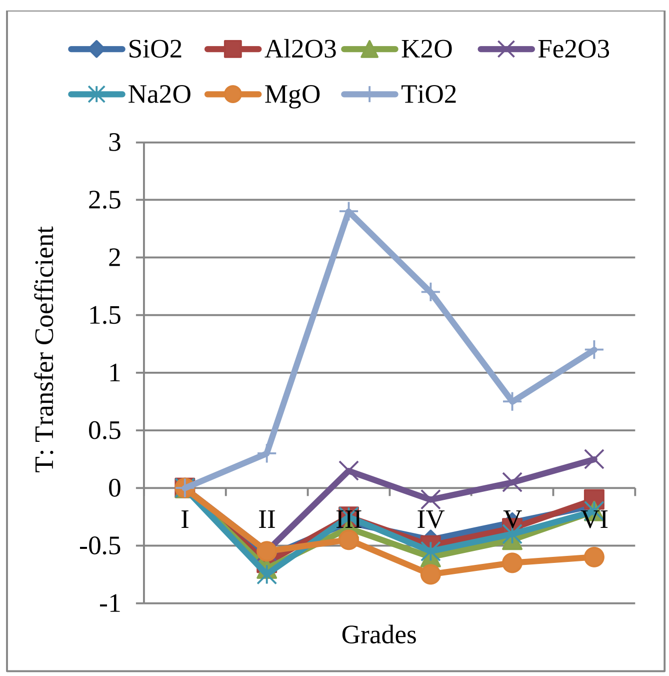

Fig. 8 The mass transfer function changes across weathering grades, reported to the fresh rock

Mass transfer calculations show deep leaching of mobile elements (e.g., Potassium K and Silicon Si) with residual enrichment of immobile elements (e.g., iron Fe and Aluminum Al).

These results record a gradual chemical evolution of the material. Weathering dominated by leaching becomes increasingly pronounced towards the most weathered levels and leads to the formation of a grade VI residual soil.

4.5. Kinematic Analysis and Domain of Applicability of Structure-Controlled Failure

The kinematic analysis was applied as a geometrical filter to the different slope faces. The admissibility of planar and wedge sliding varies significantly between slope sections (Table 1).

Slope A is highly admissible in terms of kinematics for both planar and wedge sliding, which is compatible with the observed disorder on this slope. Although slope B shows low admissibility for planar sliding and high admissibility for wedge sliding, field observations show that this slope behaves as a globally stable slope, with only a few block detachments. Slope C displays very low admissibility for planar sliding and moderate admissibility for wedge sliding, whereas field observations show rotational sliding.

The observed differences between kinematic admissibility and observed failure reveal that geometric compatibility is a necessary condition for structure-controlled failure, but that it alone does not determine its occurrence.

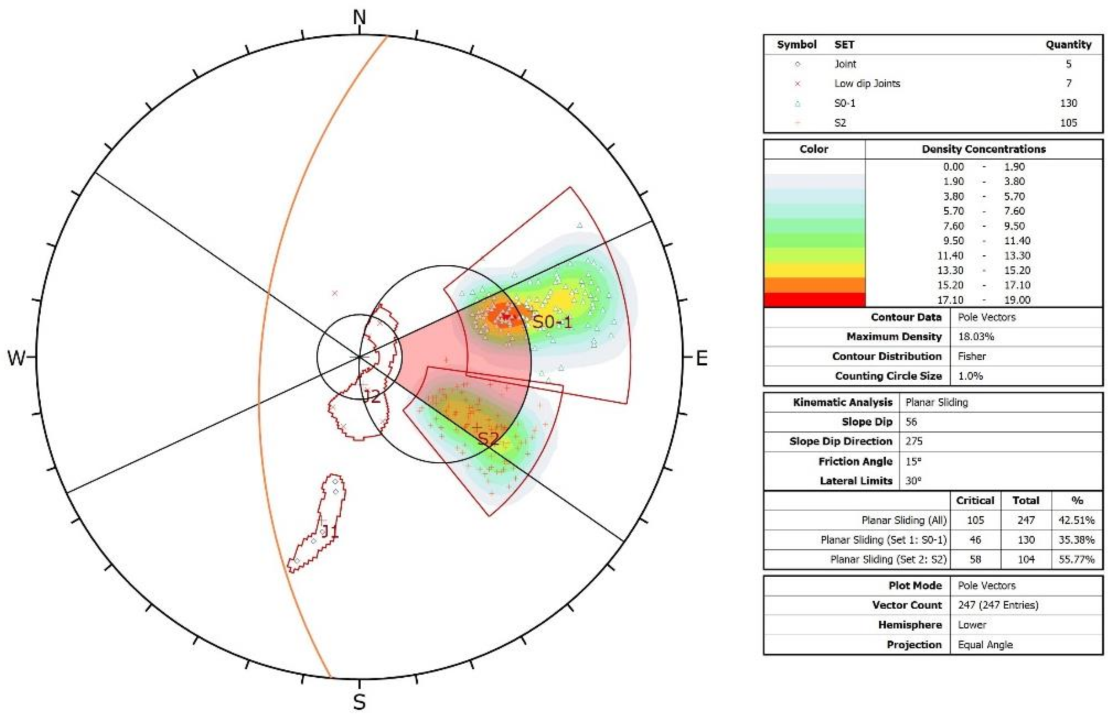

Fig. 9 Representative stereonet showing kinematic analysis of planar rupture mode in slope A

Together, field observation, laboratory characterization, and geometrical admissibility analysis allow the identification of three distinct behavioral domains associated with progressive weathering of the schist. In the fresh to slightly weathered domain, the rock mass remains structurally preserved, and slope behavior is potentially governed by discontinuity geometry. Kinematic admissibility is frequently satisfied in this domain (Figure 9); however, failure may be inhibited by joint tightening. This domain is where rock strength and discontinuity conditions remain controlling. An intermediate, moderately weathered domain marks a transitional mechanical state. Here, kinematic admissibility may exist locally but does not systematically lead to observable instabilities, highlighting a regime in which geometrical compatibility alone is no longer sufficient to predict slope instability. This domain is characterized by comparable proportions of rock cores and resulting soil, reflecting an unlocked rock mass structure, allowing a partial mobilization of rock cores within the soil matrix. The mechanical response is therefore heterogeneous, owing to the coexistence of relatively intact blocks embedded in a degraded matrix, leading to dispersed behavior and a progressive loss of predictive capability by purely geometrical models. The highly weathered domain corresponds to a matrix-controlled mechanical domain, and observed instabilities developed independently of discontinuity geometry. Kinematics is no longer applicable, and slope behavior is controlled by the mechanical properties of the weathered matrix.

Table 1. Results of the kinematic analysis for the three slope sections, including the percentage of discontinuity planes favoring planar sliding, the percentage of plane intersections favoring wedge sliding, and the types of instabilities documented during field observations

Slope	Dip/Dip Direction	Planar Sliding	Wedge Sliding	Observed Instability
A	56°/275°	47%	56%	
B	59°/303°	16%	58%	Minor block detachments
C	56°/ 355°	1.5%	35%	

4.6. Discussion

Traditional kinematic analyses evaluate slope failure potential primarily through geometric compatibility between discontinuity sets and slope orientation, generally assuming intact or homogeneous mechanical behavior. However, in weathered rock masses, the gradual degradation of strength and microstructural deterioration can significantly alter susceptibility to failure without necessarily changing geometric admissibility.

As weathering progresses, mineral transformation, microfracturing, and geochemical leaching gradually lead to a weakening of the rock mass, which alters its mechanical response and fracture mechanics [17, 34].

The present approach integrates probabilistic kinematic assessment with independently quantified weathering indices, including the Micropetrographic Index (Ip), porosity, bulk density, Schmidt rebound index, and geochemical indicators derived from volume change and mass-balance analyses. This coupling allows multi-scale interpretation of the instability conditions by relating the geometry of discontinuities with progressive degradation of material.

Rather than replacing existing kinematic techniques, the proposed framework complements their diagnostic power by highlighting zones where geometric conditions alone are insufficient to explain the observed failures. Recent studies on weathered rock profiles have also revealed relationships between microstructural degradation induced by weathering and mechanical weakening, where mineral alteration and fabric degradation gradually transform solid cohesive rock into soil-like materials with decreasing strength and stiffness [35]. Consequently, the transitional mechanical domain is defined as the transition between weathering zones 3 and 4, during which discontinuity-controlled mechanisms gradually shift to matrix-driven deformation.

At this level, test indices show remarkable changes, namely an increase in porosity and a decrease in density, micropetrological index, and geochemical leaching, indicating the gradual collapse of the original structure, to be replaced by a clay- and oxide-rich matrix. Also, dispersed strength and more complex failure behavior are observed, demonstrating the rock mass mechanical behavior transformation. A comparable rock-soil transition behavior has been described in weathered rock profiles where solid rock structures coexist with soil-like matrix properties [36].

From an engineering perspective, the results enable the definition of a practical process for assessing slope stability on weathered schist terrain.

4.6.1. Field Identification of Weathering Zones

Detailed geological mapping should distinguish weathering zones based on structural preservation, fracture density, and material coherence. Particular attention should be paid to the mechanical transition zone (zones 3-4), where rock- and soil-like characteristics coexist.

4.6.2. Multi-Scale Material Characterization

Conventional laboratory techniques, including porosity and density, micropetrographic index, and volume- and mass-balance calculations, should be used to analyze representative samples from each weathering zone to obtain physical, petrographic, and geochemical indices. This allows quantification of microstructural degradation and identification of the threshold associated with mechanical transition.

4.6.3. Coupled Kinematic Assessment.

Probabilistic kinematic analysis is only suitable for coherent rock domains where behavior controlled by discontinuities predominates. In transition zones and highly weathered zones, this interpretation must be modified, as the loss of cohesion and the development of the matrix lead to a gradual reduction in the reliability of purely geometric admissibility.

4.6.4. Identification of Transitional Mechanical Domains

Zones displaying strong dispersion in mechanical or physical properties, decreasing Ip values, and increasing porosity should be interpreted as transitional domains. These areas represent zones of elevated mechanical uncertainty and may require more conservative stability assessments.
Adaptation of modeling strategies.

The modelling methods should be chosen according to the nature of the weathering domain. In coherent rock domains, kinematic analysis and structure-based models are applicable; in transition zones, hybrid solutions combining discontinuity and weak models are more suitable; while soil mechanics-based models are recommended for highly decomposed materials. From a methodological perspective, the improvement relative to conventional approaches lies primarily in the integration of weathering indices with kinematic probability analysis.

Traditional kinematic analyses identify numerous geometrically admissible failure configurations, without providing any insight as to why some slopes fail while others hold up under the same structural conditions. By incorporating quantitative indicators of weathering-induced material degradation, the present approach provides a more physically consistent interpretation of instability processes and enables identification of zones where structural geometry alone cannot account for observed failures. Since the Schmidt hammer shows limitations in advanced stages of deterioration, additional mechanical indicators may also be necessary to characterize heavily decomposed materials fully. Pocket penetrometers or vane shear devices may afford reasonable estimates of strength parameters in soil-like materials. In situ shear testing could additionally enhance the characterization of matrix-dominated domains. Although such tests were not performed in the present study, acknowledging their relevance highlights the methodological boundaries of rebound-based indices and suggests directions for future experimental work.

Beyond static characterization, slope stability in weathered schist terrain must be considered in a time-dependent framework. Progressive weathering induces continuous changes in mineralogy, structure, porosity, and hydromechanical properties after rock exposure, causing a gradual deterioration in rock strength and stiffness [17, 35]. Hydrological processes are crucial in this evolution: the infiltration of rain or groundwater increases pore pressures, accelerates mineral alteration, and enhances microfracture propagation, promoting mechanical degradation and instability [37, 38].

These evolving conditions may generate measurable early-warning indicators of instability. Increasing dispersion in mechanical indices such as Schmidt rebound or UCS values, expansion of matrix-dominated zones, changes in hydraulic response, or progressive deformation patterns can provide signals of ongoing weakening before large-scale slope failure. Monitoring these parameters, therefore, offers a practical means of detecting early stages of instability in weathered rock masses. Engineering implications: This workflow allows practitioners to choose the most suitable method for stability analysis, and helps in early detection of transitional mechanical domains that may serve as a valuable screening tool to prioritize monitoring programs, drainage control, and reinforcement interventions in infrastructure developed over weathered schist terrains.

Finally, the results can be synthesized into a conceptual framework describing the progressive evolution of weathered schist slopes. Initially, coherent rock masses are controlled by structural discontinuities, and slope instability is governed by geometric compatibility [39]. As weathering progresses, minerals change, microfractures appear, and geochemical leaching gradually weakens the rock mass, contributing to the development of a transitional rock-soil domain in which relict structures remain, but mechanical behavior is increasingly controlled by a clay-rich matrix [34, 36]. At this level, instability mechanisms evolve from plane or wedge failures controlled by discontinuities to more complex rotational failures controlled by the matrix. Recognizing this transition from structure-controlled to matrix-dominated behavior will improve our understanding of the instability of weathered rock masses and enhance the technical assessment and long-term management of slopes.

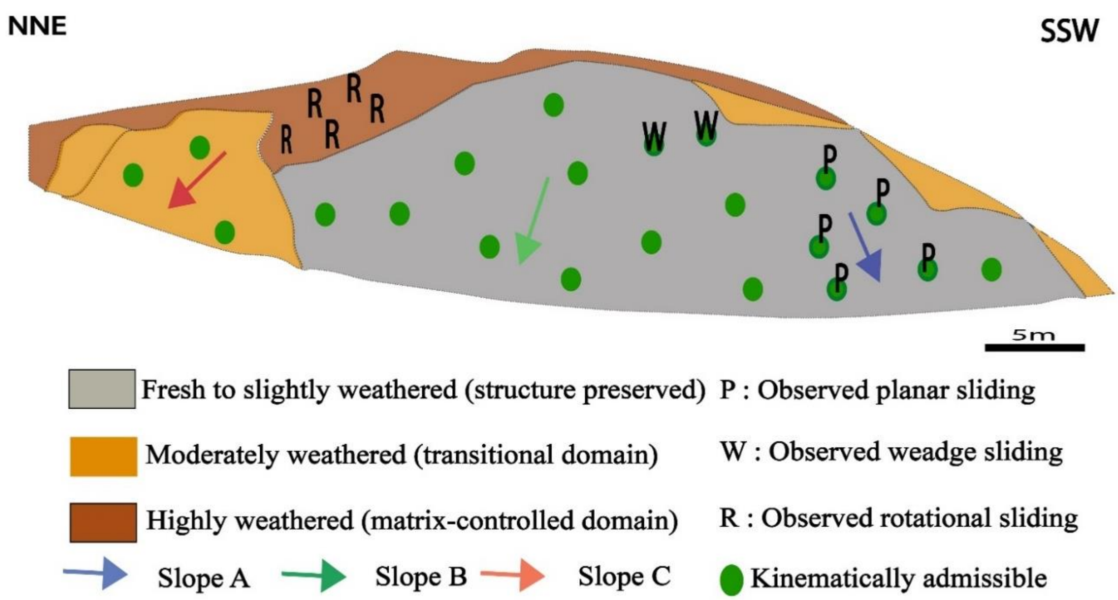

Fig. 10 Spatial comparison between kinematic admissibility and observed slope instabilities across weathering domains. Green symbols indicate slope sectors kinematically admissible for planar or wedge sliding under a fully rocky assumption, while observed failure types are indicated independently. Agreement between admissibility and observed failures is mainly restricted to moderately weathered domains. In contrast, fresh domains remain largely stable despite admissibility, and highly weathered domains exhibit matrix-controlled failures outside the applicability of kinematic analysis

Table 2. Multi-scale correlation between weathering zones, weathering grades, and associated mechanical and kinematic behavior

Weathering Zones	Rebound Index	Associated Weathering Grades	Porosity (%)	Density (Kg/m^3)	Ip	Mechanical behavior	Dominant rupture mechanism	Kinematic applicability
Zone 1	26-30	Fresh rock (I)	Low (4 -9)	High (2.58 -2.48)	High	Structurally controlled rock mass	Planar and wedge sliding along discontinuities	Satisfied
Zone 2	18-20	Fresh to slightly weathered rock (Grades I–II)			Moderate	Structurally controlled rock mass	Planar and wedge sliding along discontinuities	Satisfied
Zone 3	10-16	Moderately to highly weathered rock (Grades III–IV)	Moderate (12-19)	Decreasing (2.36-2.19)	Low	Transition to matrix-controlled domain	Mixed block detachment and matrix-assisted displacement	Locally admissible
Zone 4	Not measurable (<10)	Completely weathered rock (V)			Low	Transition to matrix-controlled domain	Mixed block detachment with increasing matrix deformation	Locally admissible
Zone 5 -6	Not measurable (<10)	Residual soils (VI)	High (≥27)	Low (1.94-1.63)	Null	Matrix-governed behavior	Soil-like failure	Not - applicable

5. Conclusion

This study provides a characterization of the weathering progression in Silurian schists at the Tamrabet site to define the transitional mechanical domain marking the shift from coherent, structurally controlled rock behavior to soil-like, matrix-governed deformation. Integrating rock mass investigation with the measurement of physical, geochemical, and petrographic properties of the rock material, the results demonstrate that the transition between weathering zones 3 and 4, encompassing material weathering grades from III to VI, represents a fundamental mechanical threshold in the evolution of schist.

Across this threshold, increasing porosity, decreasing bulk density, loss of primary minerals, negative mass-transfer coefficients for mobile elements, and a sharp decrease of the Micropetrographic Index collectively indicate the collapse of the original schist microfabric and the emergence of a swelled clay and oxide-rich matrix. When expressed at the rock mass scale, the coexistence of different weathering grades in appropriate proportions produces a transitional mechanical regime, observed in the field as a shift from discontinuity-controlled planar and wedge instabilities to rotational failures developing within the highly decomposed matrix. In this soil–rock transition, the mechanical resistance response becomes widely dispersed, and rupture behavior becomes increasingly complex.

As demonstrated by the kinematic analysis performed across the different weathering domains, although multiple sets of discontinuities result in a variety of geometrically possible failure configurations, with increased weathering and pervasive fracturing, the orientation of discontinuities becomes less influential. This evolution reflects the dominant influence of the loss of material cohesion induced by weathering, a parameter that is not considered in purely geometric kinematic models. The results, therefore, characterize an upper limit of applicability for structure-based slope stability approaches in weathered schists.

Overall, the integrated dataset reveals a coherent weathering pathway in which microstructural breakdown, geochemical leaching, mineral destabilization, and the development of swelling fines act together to govern the mechanical evolution of the rock mass and its failure mechanisms. By using weathering quantification indices coupled with probabilistic kinematic assessment, instability conditions are understood more accurately than in approaches based strictly on structural geometry. This multi-scale framework improves understanding of the transition processes between rock and soil and also provides a more solid basis for assessing stability in weathered shale terrain, where standard rock or soil models are often inadequate.

Although the integrated approach is robust, certain limitations must be acknowledged. The number of samples per weathering grade is still limited, which restricts the formal application of inferential statistical tests and may affect the estimation of intra-degree variability.

The kinematic analysis was limited to satisfying only the geometric eligibility criteria and did not consider strength parameters, quantification of cohesion loss, or hydromechanical coupling, which can have a significant influence on the response of slopes in higher degrees of weathering. Moreover, the study is focused on a single representative site in Silurian schists. Although the identified mechanical transition threshold appears internally consistent, its transferability to other lithologies, climatic conditions, or tectonic contexts requires further validation.

Future research should build on the current framework by incorporating time-dependent weathering processes, progressive strength reduction, and hydromechanical interactions into slope stability models. New paradigms should not consider stability as a fixed condition at the time of investigation or construction, but rather account for the progressive changes in material properties and structural configuration that govern long-term performance.

Transitional mechanical domains, where heterogeneous proportions of rock and soil and dispersed mechanical responses provide early indicators of a shift toward matrix-controlled failure, deserve special attention in terms of identification and monitoring. Applying this approach to other lithological contexts and validating it through long-term monitoring would enable a more rigorous assessment of the generality and predictive power of the proposed threshold concept.

This integrated knowledge can not only improve understanding of the behavior of weathered rock masses but also contribute to the development of improved classification systems adapted to transitional rock masses, better capturing the shift from discontinuity-controlled behavior to matrix-dominated deformation and providing more reliable guidance for early-stage assessment, engineering design, and long-term slope management in weathered terrains.

References

[1] Adrien Millies-Lacroix, “Landslides. Presentation of a Predictive Map of Mass Movements in the Rif (Northern Morocco),” *Mines et Géologie*, vol. 27, pp. 45-55, 1968. [Google Scholar]

[2] Khalid Margaa, and Ahmed Abdelgader, “A Methodology for Mapping Potentially Unstable Areas: Application to the Al Hoceima Region (Morocco),” *Canadian Geotechnical Journal*, vol. 35, no. 3, pp. 460-470, 1998. [CrossRef] [Google Scholar] [Publisher Link]

[3] Omar Azzouz, Bouchta El Fellah, and Ahmed Chalouan, “Landslide Processes in the Bokoya Massif (Inner Rif, Morocco) : The Example of Cala Bonita,” *Bulletin of the Scientific Institute, Rabat, Earth Sciences Section*, vol. 24, pp. 33-40, 2002. [Google Scholar]

[4] P. Olivier, “*Geological and Structural Study of the Region of Jebha (Rif, Morocco). the Termination of the Accident of Jebha-Chrafate*,” Ph. D. Dissertation, Paul Sabatier University of Toulouse, 1978. [Google Scholar] [Publisher Link]

[5] Ahmed Chalouan, and André Michard, “The Ghormarides Nappes, Rif Coastal Range, Morocco: A Variscan Chip in the Alpine Belt,” *Tectonics*, vol. 9, no. 6, pp. 1565-1583, 1990. [CrossRef] [Google Scholar] [Publisher Link]

[6] Ali Faleh, and Abdelhamid Sadiki, " Rotational Landslide at Dhar El Harrag: Example of Ground Instability in the Central Pre-Rif (Morocco)," *Bulletin of the Scientific Institute, Rabat, Earth Sciences Section*, vol. 24, pp. 41-48, 2002. [Google Scholar]

[7] H. Harmouzi et al., "Geomorphological and Geological Analysis of Akchour Landslide (Rif, Morocco). Analyse Géomorphologique et Géologie Du Glisse De Terrain D'akchour (Rif, Maroc)," *Geo-Eco-Trop*, vol. 42, no. 1, pp. 19-31, 2018. [Google Scholar]

[8] Jamal El Khattabi, and Erick Carlier, "Tectonic and Hydrodynamic Control of Landslides in the Northern Area of the Central Rif, Morocco," *Engineering Geology*, vol. 71, no. 3-4, pp. 255-264, 2004. [CrossRef] [Google Scholar] [Publisher Link]

[9] Mohamed Mastere, "*Susceptibility to Landslides in the Province of Chefchaouen (Central Rif, Morocco)*," Dissertation. University of Western Brittany-Brest, 2011. [Google Scholar] [Publisher Link]

[10] Haytam Tribak, Muriel Gasc-Barbier, and Abdelkader El Garouani, "Assessment of Ground Instabilities' Causative Factors using Multivariate Statistical Analysis Methods: Case of the Coastal Region of Northwestern Rif, Morocco," *Geosciences*, vol. 12, no. 10, pp. 1-25, 2022. [CrossRef] [Google Scholar] [Publisher Link]

[11] Hasnaa Harmouzi et al., "Landslide Susceptibility Mapping of the Mediterranean Coastal Zone of Morocco Between Oued Laou and El Jebha using Artificial Neural Networks (ANN)," *Arabian Journal of Geosciences*, vol. 12, no. 22, 2019. [CrossRef] [Google Scholar] [Publisher Link]

[12] Milton Assis Kanji, "Critical Issues in Soft Rocks," *Journal of Rock Mechanics and Geotechnical Engineering*, vol. 6, no. 3, pp. 186-195, 2014. [CrossRef] [Google Scholar] [Publisher Link]

[13] T. Le Cor et al., "Physical and Mechanical Characterization of Weak Schistose Rocks," *ISRM International Symposium - EUROCK 2013*, Wroclaw, Poland, pp. 1-6, 2013. [Google Scholar] [Publisher Link]

[14] Claude Saint-Leu, Jacques Lerau, and Pierre Sirieys, "Fracture Mechanisms of the Lacaune Schists (Tarn). Influence of Isotropic Pressure," *Bulletin of Mineralogy*, vol. 101, no. 4, pp. 437-441, 1978. [Google Scholar] [Publisher Link]

[15] Milene Sabino Lana, "Some Reflections About Engineering Behavior of Schists and Phyllites in Brazil," *ISRM 2nd International Specialized Conference on Soft Rocks*, Cartagena, Colombia, 2016. [Google Scholar] [Publisher Link]

[16] M.F. Leão, and E.A.G. Marques, "Morphology and Geotechnical Characterization of a Phyllite Weathering Profile Developed Under Tropical Climate," *5th International Conference on Geotechnical and Geophysical Site Characterization*, Gold Coast, QLD, Australia, pp. 1-5, 2016. [Google Scholar]

[17] Peter George Fookes, William Robert Dearman, and John Allan Franklin, "Some Engineering Aspects of Rock Weathering with Field Examples from Dartmoor and Elsewhere," *Quarterly Journal of Engineering Geology and Hydrogeology*, vol. 4, no. 3, pp. 139-185, 1971. [CrossRef] [Google Scholar] [Publisher Link]

[18] H. Robert G.K. Hack, *Weathering, Erosion, and Susceptibility to Weathering*, Soft Rock Mechanics and Engineering, Springer, Cham, pp. 291-333, 2019. [CrossRef] [Google Scholar] [Publisher Link]

[19] Shintaro Yamasaki, and Masahiro Chigira, "Weathering Mechanisms and their Effects on Landsliding in Pelitic Schist," *Earth Surface Processes Landforms*, vol. 36, no. 4, pp. 481-494, 2011. [CrossRef] [Google Scholar] [Publisher Link]

[20] Bhawani Singh, and R.K. Goel, *Engineering Rock Mass Classification: Tunneling, Foundations, and Landslides*, Elsevier, 2012. [CrossRef] [Google Scholar] [Publisher Link]

[21] M. de Souza, "Slope Stability in Road Infrastructure Civil Engineering," *Técnico Lisboa*, 2017. [Google Scholar]

[22] Mário Quinta-Ferreira et al., "Cut Slopes Failures on the Triassic Beds in Coimbra, Portugal," *Bulletin of Engineering Geology and the Environment*, vol. 72, no. 3-4, pp. 383-396, 2013. [CrossRef] [Google Scholar] [Publisher Link]

[23] J. Kornprobst et al., " Geological map of the Rif. Talembote. Scale 1:50,000," Notes and Memoirs of the Geological Survey of Morocco, 1975. [Google Scholar]

[24] J. Kornprobst, and Durand Delga, M, "Geological Map of the Rif. NI-30-XIX-4ab, Tetouan - Ras Mazari / Kingdom of Morocco, Industrial and Cooperation Studies Office France, Rabat, Morocco, Geological Survey; 1985. [Google Scholar]

[25] R.P. Martin, and S.R. Hencher, "Principles for Description and Classification of Weathered Rock for Engineering Purposes," *Geological Society, London, Engineering Geology Special Publications*, vol. 2, no. 1, pp. 299-308, 1986. [CrossRef] [Google Scholar] [Publisher Link]

[26] David J. Varnes, "Slope Movement Types and Processes," *Special Report*, vol. 176, no. 11, pp. 11-33, 1978. [Google Scholar]

[27] Adnan Aydin, *ISRM Suggested Method for Determination of the Schmidt Hammer Rebound Hardness: Revised Version*, The ISRM Suggested Methods for Rock Characterization, Testing and Monitoring: 2007-2014, Springer, Cham, pp. 25-33, 2014. [CrossRef] [Google Scholar] [Publisher Link]

[28] Prayag Maharjan, "Texture and Index Properties of Rocks from Malekhu-Thopal Khola Area, Central Nepal Lesser Himalaya," *Bulletin of the Department of Geology*, vol. 18, pp. 1-14, 2015. [CrossRef] [Google Scholar] [Publisher Link]

[29] R. Ulusay, *The ISRM Suggested Methods for Rock Characterization, Testing and Monitoring: 2007-2014*, 1st ed., Springer Cham, 2015. [CrossRef] [Google Scholar] [Publisher Link]

[30] Afnor Editions, NF P 94-410-3 : Rocks - Tests for Determining the Physical Properties of Rocks - Part 3 : Determination of Porosity, 2001. [Online]. Available: https://www.boutique.afnor.org/fr-fr/norme/nf-p944103/roches-essais-pour-determiner-les-proprietes-physiques-des-roches-partie-3-/fa106661/18531

[31] Afnor Editions, NF P94-064 : Reconnaissance and Testing - Dry Density of a Rock Element - Hydrostatic Weighing Method, 1993. [Online]. Available: https://www.boutique.afnor.org/fr-fr/norme/nf-p94064/sols-reconnaissance-et-essais-masse-volumique-seche-dun-element-de-roche-me/fa028330/11064

[32] George H. Brimhall, Charles N. Alpers, and Aric B. Cunningham, "Analysis of Supergene Ore-Forming Processes and Ground-Water Solute Transport using Mass Balance Principles," *Economic Geology*, vol. 80, no. 5, pp. 1227-1256, 1985. [CrossRef] [Google Scholar] [Publisher Link]

[33] T.Y. Irfan, and W.R. Dearman, "The Engineering Petrography of a Weathered Granite in Cornwall, England," *Quarterly Journal of Engineering Geology*, vol. 11, no. 3, pp. 233-244, 1978. [CrossRef] [Google Scholar] [Publisher Link]

[34] J.C. Cripps, and R.K. Taylor, "The Engineering Properties of Mudrocks," *Quarterly Journal of Engineering Geology and Hydrogeology*, vol. 14, no. 4, pp. 325-346, 1981. [CrossRef] [Google Scholar] [Publisher Link]

[35] Yizhao Wang et al., "Study on the Mechanical Properties and Microscopic Evolution Mechanisms of Weathered Granite Soil," *Scientific Reports*, vol. 14, no. 1, pp. 1-16, 2024. [CrossRef] [Google Scholar] [Publisher Link]

[36] Duan Swart, and Matthys A. Dippenaar, "Weathering Profile of Completely Weathered Rock from the Dullstroom Formation, South Africa," *Bulletin of Engineering Geology and the Environment*, vol. 84, no. 5, pp. 1-28, 2025. [CrossRef] [Google Scholar] [Publisher Link]

[37] Andrew Mitchell, and Oliver Sass, "Rock Weathering: The Effects of Varying Rock Moisture on Controlled Weathering Cycles in Low Porosity Limestone," *Geomorphology*, vol. 457, pp. 1-15, 2024. [CrossRef] [Google Scholar] [Publisher Link]

[38] Muhammad Fathur Rouf Hasan et al., "Influence of Rock Weathering and Saturation on Compressive Strength and Slope Stability: A Uniaxial Test Analysis," *International Journal of Safety and Security Engineering*, vol. 14, no. 1, pp. 145-153, 2024. [CrossRef] [Google Scholar] [Publisher Link]

[39] John A. Hudson, and John P. Harrison, *Engineering Rock Mechanics: An Introduction to the Principles*, 1st ed., Elsevier,1997. [Google Scholar] [Publisher Link]